European Radiology (2023) 33:4668–4675
https://doi.org/10.1007/s00330-023-09434-1

European Radiology
EUROPEAN SOCIETY OF RADIOLOGY

CARDIAC

Radiation dose optimization for photon-counting CT coronary artery calcium scoring for different patient sizes: a dynamic phantom study

Magdalena M. Dobrolinska[1,2,3] · Niels R. van der Werf[3] · Judith van der Bie[3] · Joël de Groen[3] · Marcel Dijkshoorn[3] · Ronald Booij[3] · Ricardo P. J. Budde[3] · Marcel J. W. Greuter[1,4] · Marcel van Straten[3]

Received: 19 October 2022 / Revised: 19 October 2022 / Accepted: 7 January 2023 / Published online: 2 February 2023

Abstract

Purpose To systematically assess the radiation dose reduction potential of coronary artery calcium (CAC) assessments with photon-counting computed tomography (PCCT) by changing the tube potential for different patient sizes with a dynamic phantom.

Methods A hollow artery, containing three calcifications of different densities, was translated at velocities corresponding to 0, < 60, 60–75, and > 75 beats per minute within an anthropomorphic phantom. Extension rings were used to simulate average- and large -sized patients. PCCT scans were made with the reference clinical protocol (tube potential of 120 kilovolt (kV)), and with 70, 90, Sn100, Sn140, and 140 kV at identical image quality levels. All acquisitions were reconstructed at a virtual monoenergetic energy level of 70 keV. For each calcification, Agatston scores and contrast-to-noise ratios (CNR) were determined, and compared to the reference with Wilcoxon signed-rank tests, with $p < 0.05$ indicating significant differences.

Results A decrease in radiation dose (22%) was achieved at Sn100 kV for the average-sized phantom. For the large phantom, Sn100 and Sn140 kV resulted in a decrease in radiation doses of 19% and 3%, respectively. Irrespective of CAC density, Sn100 and 140 kVp did not result in significantly different CNR. Only at Sn100 kV were there no significant differences in Agatston scores for all CAC densities, heart rates, and phantom sizes.

Conclusion PCCT at tube voltage of 100 kV with added tin filtration and reconstructed at 70 keV enables a ≥ 19% dose reduction compared to 120 kV, independent of phantom size, CAC density, and heart rate.

Key Points

- *Photon-counting CT allows for reduced radiation dose acquisitions (up to 19%) for coronary calcium assessment by reducing tube voltage while reconstructing at a normal monoE level of 70 keV.*
- *Tube voltage reduction is possible for medium and large patient sizes, without affecting the Agatston score outcome.*

Keywords X-ray computed tomography · Calcium · Coronary vessels · Imaging phantoms

Magdalena M Dobrolinska and Niels R van der Werf shared first authorship.

Magdalena M Dobrolinska and Niels R van der Werf contributed equally to this work.

✉ Niels R. van der Werf
nrvdwerf@gmail.com

1 Department of Radiology, University Medical Center Groningen, University of Groningen, Groningen, The Netherlands

2 Division of Cardiology and Structural Heart Diseases, Medical University of Silesiain, Katowice, Katowice, Poland

3 Department of Radiology & Nuclear Medicine, Erasmus University Medical Center, Rotterdam, The Netherlands

4 Department of Robotics and Mechatronics, University of Twente, Enschede, The Netherlands

Abbreviations

ATCM	Automatic tube current modulation
CAC	Coronary artery calcium
CNR	Contrast-to-noise ratio
$CTDI_{vol}$	Volumetric CT dose index
HA	Hydroxyapatite
HU	Hounsfield units
keV	Kiloelectron volt
kV	Kilovolt
PCCT	Photon-counting CT
VMI	Virtual monoenergetic image

Introduction

An important step in clinical radiology is the advent of photon-counting CT [1–6]. This new technology employs smaller detector elements than conventional CT. These smaller detector elements directly convert individual incoming photons into electrical signals and register these individually in predefined energy bins, as opposed to indirect conversion which includes first the transition of photon energy to visible light after which this is converted to an electrical signal. Moreover, only integration over multiple photons was feasible with conventional CT, where PCCT allows for the detection of single photons. PCCT, therefore, has several benefits: the availability of spectral data for each CT exam, as well as increased spatial resolution, and a reduced impact of electronic noise [1, 3, 7].

As shown in ROBINSCA trial, coronary artery calcium (CAC) can be used as a screening tool to guide preventive treatment in asymptomatic individuals [8]. According to CAC's screening potential, the reduction of radiation dose of CAC scan would be especially of interest. Thanks to the availability of spectral data for each CT scan, an important use case is related to CAC quantification as this could result in reduced radiation dose [2, 9–14]. Quantification of CAC is clinically performed according to the Agatston methodology [15]. This methodology dictates the use of 120-kilovolt (kV) tube voltage for all patients, independent of patient size. As a result, a single threshold (130 Hounsfield units (HU)) can be used for CAC discrimination. However, the most efficient way to decrease radiation dose for CT is to decrease the tube voltage to patient-size–specific values [16–21]. This is especially interesting considering the increase of CT CAC assessments and its related increase in cumulative radiation dose [22]. For conventional CT, a change in tube voltage results in a change in CT numbers of CAC. To be able to use these images for CAC assessment, several solutions have been proposed to overcome any difference in CAC quantification. These solutions include specific calcium-aware reconstruction kernels or adjusted CAC scoring thresholds [16–21]. For PCCT, however, it is possible to maintain CT numbers while scanning at different tube potentials by reconstructing the same virtual monoenergetic image (VMI) level. Specifically for CAC assessments, this means data acquisition at a patient-size—specific tube potential, and reconstructing at a VMI level of 70 kiloelectron volt (keV) which corresponds to the conventional 120-kV reconstructions [12, 14, 23].

For a clinical dual-source PCCT, it was previously shown with the aid of a dynamic phantom that a tube potential of 90 kV allowed for reproducible Agatston scores for large phantom sizes in comparison with standard 120-kV acquisitions [12]. The impact on a medium-sized phantom remains unknown. This is of particular interest for an updated version of this same PCCT system, which allows for a larger variety of tube potentials (70, 90, Sn100, 120, Sn140, and 140), eligible for VMI reconstructions of 70 keV.

The aim of the current study is, therefore, to systematically assess the radiation dose reduction potential of CAC assessments at all available tube voltages with a PCCT system for different patient sizes with a dynamic phantom.

Methods

A hollow artificial artery (inner diameter 0.5 cm, outer diameter 1.1 cm) was positioned within a water compartment at the center of an anthropomorphic thorax phantom (QRM-thorax, PTW) (Fig. 1). The artery was made of solid water (0 HU) and contained three hollow cylindrical hydroxyapatite (HA) calcifications of identical dimensions (inner diameter 0.5 cm, outer diameter 1.1 cm, length 0.5 cm), but different densities. The HA densities were 200, 400, and 800 mg/cc, designated as low, medium, and high density, respectively. Both the water compartment and the inner lumen of the artery were filled with water. The artery was translated by a robotic arm (Sim2D, PTW) perpendicular to the z-axis at velocities of 0, 10, 20, and 30 mm/s, approximately equivalent to the mean in vivo motion of coronary arteries during the scan phase at heart rates of 0, < 60, 60–75, and > 75 beats per minute (bpm), respectively [24–26]. The electrocardiogram output of the robotic arm was used to ensure data acquisition during linear motion of the robot, without any turning points. To simulate average and large patient sizes, medium and large fat-tissue equivalent extension rings (M and L extension ring, PTW) were positioned around the thorax phantom increasing the outer dimensions to 350 mm × 200 mm and 400 mm × 300 mm, respectively [27].

First, the dynamic phantom was scanned on a dual-source PCCT (NAEOTOM Alpha, Siemens Healthineers) with the routinely used clinical reference protocol: tube potential 120 kV; axial scan technique; automatic tube current modulation (ATCM) with image quality level 16 (CareIQ, Siemens Healthineers), reconstruction technique filtered-back-projection (FBP or QIR off); field-of-view 220 mm; matrix 512 × 512; slice thickness/increment at 3/1.5 mm; reconstruction kernel Qr36. Second, additional acquisitions were performed for both phantom sizes at 70, 90, Sn100, Sn140, and 140 kV, at the same image quality level of 16 using ATCM that aims at keeping image noise constant while changing kV. All scans were reconstructed at a VMI level of 70 keV. Each acquisition was repeated five times, with manual repositioning of the setup between each scan (2 mm translation, 2° rotation), to introduce inter-scan variability.

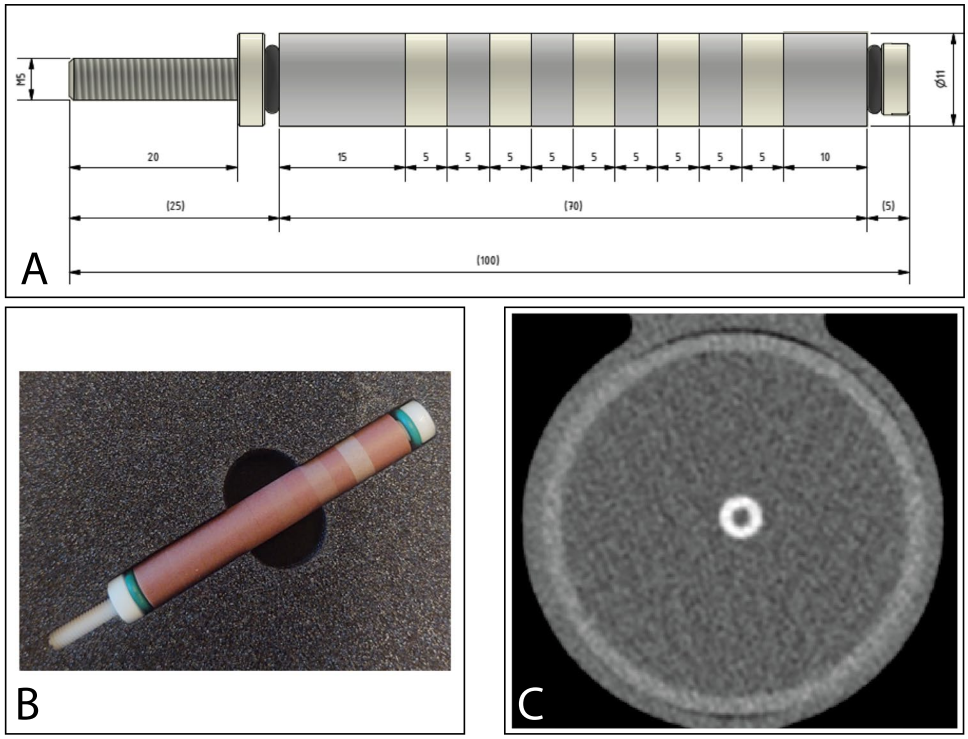

Fig. 1 Representations of the hollow artificial artery: **A** schematic overview with dimensions in millimeters, with the solid water (gray) and hydroxyapatite calcifications (yellow) indicated, (**B**) photograph, and (**C**) a 70-keV reconstructed cross-sectional image of the medium-density calcification (window width/window level at 750/90 Hounsfield units)

For each calcification, Agatston scores were automatically determined with a previously validated Python script, using CT vendor-specific CAC scoring parameters [28]. As all scans were reconstructed at a VMI level of 70 keV, the conventional Agatston threshold of 130 HU was applied. All voxels exceeding this threshold were considered to be CAC.

For each calcification density, the contrast-to-noise ratio (CNR) was determined to assess potential differences between each acquisition and the reference. With this, the influence of tube potential on signal intensity and image noise was assessed. The CNR was calculated as:

$$CNR = \frac{\left|Mean_{CAC} - Mean_{Background}\right|}{Standarddeviation_{Background}}$$

where $\mathrm{Mean}_{\mathrm{CAC}}$ was the mean CT number of all voxels exceeding the CAC scoring threshold, and $\mathrm{Mean}_{\mathrm{Background}}$ and Standard $\mathrm{deviation}_{\mathrm{Background}}$ the mean CT number and standard deviation of the CT numbers within a region-of-interest of 450 voxels (15×30) in the water compartment.

Statistical analyses were performed using SPSS version 27 (SPSS, IBM). For each tube potential, differences in CNR or Agatston score with the reference protocol values were assessed with the use of Wilcoxon signed-rank tests. *p* values below 0.05 were considered to indicate a statistically significant difference.

Results

Radiation dose

The effective tube current time products, based on the ATCM level 16, are indicated in Table 1. Reference volumetric CT dose index ($\mathrm{CTDI}_{\mathrm{vol}}$) values, retrieved from the radiation dose structured report, at 120 kV, were 2.06 and 2.78 mGy for the medium and large phantom sizes, respectively. For the medium phantom, the largest decrease in radiation dose with respect to the reference at 120 kV was achieved for Sn100-kV acquisitions, at 22% (Fig. 2). Acquisitions at 90 kV also reduced the radiation dose, while all other tube potentials increased radiation dose for medium-sized patients. For the large phantom, Sn100- and Sn140-kV

Table 1 Effective tube current time products for different tube potentials and phantom sizes

Tube potential (kV)	Effective tube current time product (mAs)	
	Medium phantom	Large phantom
120	13	18
70	90	151
90	29	43
Sn100	95	132
Sn140	29	37
140	9	13

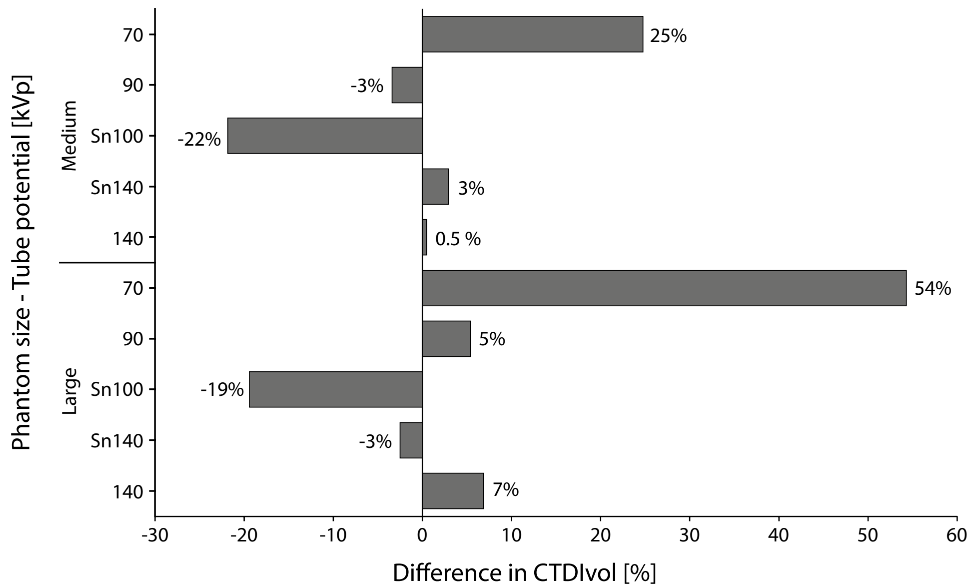

Fig. 2 For each phantom size, volumetric CT dose index ($CTDI_{vol}$) differences for all tube potentials with respect to the reference acquisition at 120 kV

acquisitions resulted in a decrease in radiation doses of 19% and 3%, respectively.

CNR

In comparison with the reference CNR of the stationary CAC for the large phantom, reference CNR were higher for the medium-sized phantom for all CAC densities (Table 2). For the low-density CAC, significantly different ($p < 0.05$) CNRs were shown for the large phantom at 70 kV, the medium phantom at 90 kV, and the medium phantom at Sn140 kV. For the medium-density CAC, only the medium-sized phantom at Sn140 kV resulted in a significantly different ($p = 0.043$) CNR in comparison with the reference. For the high-density CAC, significantly different CNR were not shown for the used tube potentials and phantom sizes.

Agatston scores

For both the low- and medium-density CAC, Agatston scores at 70 and Sn100 kV acquisitions did not show significant differences ($p > 0.05$) with the reference for all phantom sizes and heart rates (Fig. 3). For the medium-density CAC, this also applied to the 140-kV acquisitions. For the high-density CAC, only Sn140-kV acquisitions of the static CAC within the medium-sized phantom resulted in a significantly different ($p = 0.043$) Agatston score in comparison with the

Table 2 Median (total range) contrast-to-noise ratios for all tube potentials, phantom sizes, and coronary artery calcium densities at rest. Bold values indicate a significant difference from the respective phantom size and density calcification at a tube potential of 120 kV

Tube potential (kV)	Phantom size	Low density		Medium density		High density	
		CNR	*p*	CNR	*p*	CNR	*p*
120	Medium	9.2 (8.7–9.6)	Ref	14.5 (14.1–15.9)	Ref	24.8 (23.2–27.6)	Ref
	Large	7.0 (6.2–8.0)	Ref	10.9 (9.9–12.5)	Ref	18.4 (16.2–21.1)	Ref
70	Medium	8.8 (8.1–9.2)	0.138	14.6 (13.4–15.0)	0.225	23.7 (23.0–25.2)	0.500
	Large	8.0 (7.6–9.3)	**0.043**	12.3 (11.8–13.8)	0.080	20.1 (19.2–22.4)	0.225
90	Medium	8.5 (7.6–9.0)	**0.043**	13.6 (12.1–15.0)	0.080	22.6 (21.6–25.0)	0.080
	Large	6.9 (6.0–8.0)	0.500	10.7 (9.5–12.8)	0.345	17.9 (15.6–20.6)	0.225
Sn100	Medium	8.6 (7.1–9.8)	0.225	14.5 (11.7–15.4)	0.225	24.1 (20.6–25.8)	0.138
	Large	7.1 (6.7–8.1)	0.345	11.2 (10.7–12.8)	0.345	18.1 (16.9–20.7)	0.893
Sn140	Medium	8.0 (7.1–8.3)	**0.043**	12.8 (11.6–13.9)	**0.043**	21.3 (19.9–23.8)	0.080
	Large	6.2 (5.8–6.5)	0.080	9.8 (9.6–10.3)	0.080	15.8 (15.7–16.8)	0.080
140	Medium	9.1 (8.5–9.4)	0.686	14.3 (13.5–15.2)	0.343	24.6 (22.4–25.7)	0.686
	Large	7.3 (6.9–8.3)	0.225	11.6 (10.7–13.1)	0.138	19.1 (18.0–21.9)	0.138

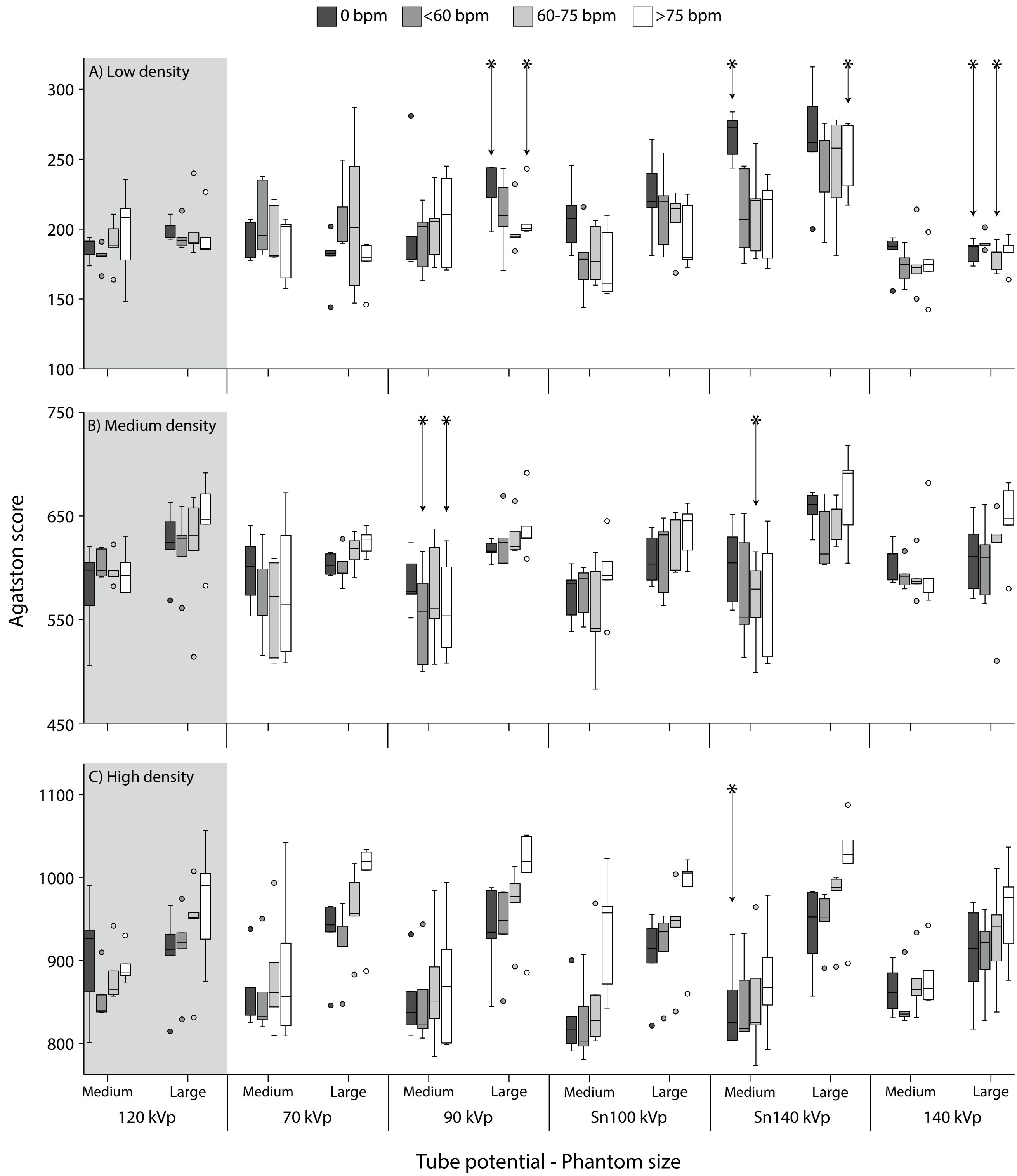

Fig. 3 Agatston scores for low (**A**), medium (**B**), and high (**C**) density coronary artery calcifications (CAC). For each CAC density, box and whisker plots are presented for all tube potentials, phantom sizes, and four heart rates. The reference acquisition (120 kV) is indicated by the gray area. For each phantom size and heart rate, significantly different Agatston scores are indicated with an asterisk

reference. For 70, 90, Sn100, and 140 kV, Agatston scores were not shown to differ significantly from the reference for the high-density CAC.

Discussion

This study has identified that employing a tube potential of Sn100 kV results in a radiation dose reduction of ≥ 19% without showing significantly different CNR or Agatston scores, independent of phantom size, CAC density, or heart rate. At other tube potentials, significant differences in CNR with the reference did not always result in significantly different Agatston scores.

Our study is the first to assess the potential of tube voltage–independent calcium scoring for dynamic CAC in different patient sizes. In a static phantom study, Mergen et al found accurate Agatston scores (≤ 5% percentage deviation with conventional CT) for 90- and Sn100-kV acquisitions independent of phantom size [29]. Their study, however, did not assess interscan variability, with only 1 scan per acquisition and reconstruction combination. For our study, with 5 repeated measurements, significant differences in Agatston scores were shown for at least one CAC density for acquisitions at 90 kV. Finally, as a lower standard ATCM level was used, our study indicated smaller levels of radiation dose reduction in comparison with the reference clinical protocol at 120 kV. Van der Werf et al previously found a radiation dose reduction potential of 57% for dynamic medium- and high-density CAC when acquiring data at 90 kV with reduced tube current levels [12]. In our current study, which employed differently shaped calcifications, however, 90 kV resulted in significantly different Agatston scores in comparison with the reference for low- and medium-density CAC. For Sn100 kV, significant differences with the reference were not indicated, also not for low-density CAC. In our current study, we found for the large phantom slightly different radiation dose levels in comparison with the previous study [12]. We hypothesize that this difference is the result of using an updated software version of the PCCT system (VA50), differences in pitch values, and the limited reproducibility of ATCM. Nevertheless, in both studies, the radiation dose reduction was highest at Sn100 kV when using ATCM at a constant IQ level.

The ATCM used image noise to define the target IQ level. Alternatively, one might target at the CNR of CAC. Although this makes sense physically, it has drawbacks as well. It would require a new way of calcium scoring because HU numbers of CAC might change and image noise might increase resulting in falsely detected CAC. In this study, priority was given to the applicability of the conventional Agatston scoring methodology.

According to clinical guidelines, CAC should be taken into consideration when planning lipid-lowering therapy [30, 31]. Moreover, follow-up CAC scans can be applied as a monitoring of atherosclerotic disease [32]. Taking all things together, the increasing importance of CAC scanning will lead to a growing number of patients who need a CAC scan. Therefore, we should aim for clinical protocols which enable scan acquisition at a lower radiation dose. Importantly, as depicted on Fig. 2, a tube potential of Sn100 kV decreased the radiation dose in both patient sizes. In addition, as there was no difference in Agatston score between the proposed acquisition parameters and reference scan, we believe it might be applied in daily clinical practice after clinical validation.

This study has limitations. First, an anthropomorphic phantom with a hollow artificial artery was used for the current study. The outer dimensions of this phantom were needed to enable the drilling of the internal lumen. These outer dimensions (11-mm diameter) are large compared to the dimensions of in vivo calcifications. Therefore, these results need further validation in a patient study. Next, only phantom data was included in the current analysis. Clinical validation of our results is needed in advance of widespread clinical use.

To conclude, PCCT allows for a radiation dose reduction of ≥ 19% by merely changing the tube potential to Sn100 kV, without changing image quality or Agatston score outcome.

Funding The authors state that this work has not received any funding.

Declarations

Guarantor The scientific guarantor of this publication is Marcel van Straten.

Conflict of interest The Erasmus MC department of Radiology & Nuclear Medicine receives research funding from Siemens Healthcare. Niels van der Werf has been employed by Philips during the final stages of this work.
The other authors of this manuscript declare no relationships with any companies whose products or services may be related to the subject matter of the article.

Statistics and biometry No complex statistical methods were necessary for this paper.

Informed consent Not applicable.

Ethical approval Institutional Review Board approval was not required because this is a phantom-only study.

Methodology
- prospective
- experimental
- performed at one institution

References

1. Willemink MJ, Persson M, Pourmorteza A et al (2018) Photon-counting CT: technical principles and clinical prospects. Radiology 289:293–312. https://doi.org/10.1148/radiol.2018172656
2. Sandfort V, Persson M, Pourmorteza A, Noël PB, Fleischmann D, Willemink MJ (2021) Spectral photon-counting CT in cardiovascular imaging. J Cardiovasc Comput Tomogr 15(3):218–225. https://doi.org/10.1016/j.jcct.2020.12.005
3. Flohr T, Ulzheimer S, Petersilka M, Schmidt B (2020) Basic principles and clinical potential of photon-counting detector CT. Chin J Acad Radiol 3:19–34. https://doi.org/10.1007/s42058-020-00029-z
4. Leng S, Bruesewitz M, Tao S et al (2019) Photon-counting detector CT: system design and clinical applications of an emerging technology. Radiographics 39:729–743. https://doi.org/10.1148/rg.2019180115
5. Si-Mohamed S, Bar-Ness D, Sigovan M et al (2017) Review of an initial experience with an experimental spectral photon-counting computed tomography system. Nucl Instrum Methods Phys Res A 873:27–35. https://doi.org/10.1016/j.nima.2017.04.014
6. Taguchi K, Iwanczyk JS (2013) Vision 20/20: single photon counting x-ray detectors in medical imaging. Med Phys 40:100901. https://doi.org/10.1118/1.4820371
7. Ren L, Rajendran K, McCollough CH, Yu L (2019) Radiation dose efficiency of multi-energy photon-counting-detector CT for dual-contrast imaging. Phys Med Biol 64:245003. https://doi.org/10.1088/1361-6560/ab55bf
8. van der Aalst CM, Denissen SJAM, Vonder M et al (2020) Screening for cardiovascular disease risk using traditional risk factor assessment or coronary artery calcium scoring: the ROBINSCA trial. Eur Heart J Cardiovasc Imaging 21:1216–1224. https://doi.org/10.1093/ehjci/jeaa168
9. Sandstedt M, Marsh J, Rajendran K et al (2021) Improved coronary calcification quantification using photon-counting-detector CT: an ex vivo study in cadaveric specimens. Eur Radiol 31:6621–6630. https://doi.org/10.1007/s00330-021-07780-6
10. van der Werf NR, Si-Mohamed S, Rodesch PA et al (2022) Coronary calcium scoring potential of large field-of-view spectral photon-counting CT: a phantom study. Eur Radiol 32:152–162. https://doi.org/10.1007/S00330-021-08152-W
11. van der Werf N, Rodesch P, Si-Mohamed S et al (2022) Improved coronary calcium detection and quantification with low-dose full field-of-view photon-counting CT: a phantom study. Eur Radiol. https://doi.org/10.1007/s00330-021-08421-8
12. van der Werf NR, van Gent M, Booij R, et al (2021) Dose reduction in coronary artery calcium scoring using mono-energetic images from reduced tube voltage dual-source photon-counting CT data: a dynamic phantom study. Diagnostics 11. https://doi.org/10.3390/diagnostics11122192
13. Symons R, Sandfort V, Mallek M et al (2019) Coronary artery calcium scoring with photon-counting CT: first in vivo human experience. Int J Cardiovasc Imaging 35:733–739. https://doi.org/10.1007/s10554-018-1499-6
14. van der Werf NR, Greuter MJW, Booij R, van der Lugt A, Budde RPJ, van Straten M (2022) Coronary calcium scores on dual-source photon-counting computed tomography: an adapted Agatston methodology aimed at radiation dose reduction. Eur Radiol 32(8):5201–5209. https://doi.org/10.1007/S00330-022-08642-5
15. Agatston AS, Janowitz WR, Hildner FJ et al (1990) Quantification of coronary artery calcium using ultrafast computed tomography. J Am Coll Cardiol 15:827–832. https://doi.org/10.1016/0735-1097(90)90282-T
16. Booij R, van der Werf NR, Budde RPJ et al (2020) Dose reduction for CT coronary calcium scoring with a calcium-aware image reconstruction technique: a phantom study. Eur Radiol 30:3346–3355. https://doi.org/10.1007/s00330-020-06709-9
17. van der Werf NR, Booij R, Schmidt B et al (2021) Evaluating a calcium-aware kernel for CT CAC scoring with varying surrounding materials and heart rates : a dynamic phantom study. Eur Radiol 31:9211–9220. https://doi.org/10.1007/s00330-021-08076-5
18. Vingiani V, Abadia AF, Schoepf UJ et al (2020) Low-kV coronary artery calcium scoring with tin filtration using a kV-independent reconstruction algorithm. J Cardiovasc Comput Tomogr 14:246–250. https://doi.org/10.1016/j.jcct.2019.11.006
19. Vingiani V, Abadia AF, Schoepf UJ et al (2020) Individualized coronary calcium scoring at any tube voltage using a kV-independent reconstruction algorithm. Eur Radiol 30(11):5834–5840. https://doi.org/10.1007/s00330-020-06951-1
20. Tao S, Sheedy E, Bruesewitz M et al (2021) Technical Note: kV-independent coronary calcium scoring: a phantom evaluation of score accuracy and potential radiation dose reduction. Med Phys 48:1307–1314. https://doi.org/10.1002/mp.14663
21. Marwan M, Mettin C, Pflederer T et al (2013) Very low-dose coronary artery calcium scanning with high-pitch spiral acquisition mode: comparison between 120-kV and 100-kV tube voltage protocols. J Cardiovasc Comput Tomogr 7:32–38. https://doi.org/10.1016/j.jcct.2012.11.004
22. Mahabadi AA, Möhlenkamp S, Lehmann N et al (2017) CAC score improves coronary and CV risk assessment above statin indication by ESC and AHA/ACC Primary Prevention Guidelines. JACC Cardiovasc Imaging 10:143–153. https://doi.org/10.1016/j.jcmg.2016.03.022
23. Eberhard M, Mergen V, Higashigaito K, et al (2021) Coronary calcium scoring with first generation dual-source photon-counting CT-first evidence from phantom and in-vivo scans. Diagnostics (Basel) 11:. https://doi.org/10.3390/DIAGNOSTICS11091708
24. Husmann L, Leschka S, Desbiolles L et al (2007) Coronary artery motion and cardiac phases: dependency on heart rate—implications for CT image reconstruction. Radiology 245:567–576
25. van der Werf NR, Willemink MJ, Willems TP et al (2017) Influence of heart rate on coronary calcium scores: a multi-manufacturer phantom study. Int J Cardiovasc Imaging 34:959–966. https://doi.org/10.1007/s10554-017-1293-x
26. Achenbach S, Ropers D, Holle J et al (2000) In-plane coronary arterial motion velocity: measurement with electron-beam CT. Radiology 216:457–463. https://doi.org/10.1148/radiology.216.2.r00au19457
27. McCollough CH, Ulzheimer S, Halliburton SS et al (2007) Coronary artery calcium: a multi-institutional, multimanufacturer international standard for quantification at cardiac CT. Radiology 243:527–538. https://doi.org/10.1148/radiol.2432050808
28. Praagh GD, Werf NR, Wang J et al (2021) Fully automated quantification method (FQM) of coronary calcium in an

anthropomorphic phantom. Med Phys 48:3730–3740. https://doi.org/10.1002/mp.14912
29. Mergen V, Higashigaito K, Allmendinger T et al (2021) Tube voltage-independent coronary calcium scoring on a first-generation dual-source photon-counting CT—a proof-of-principle phantom study. Int J Cardiovasc Imaging 2021:1–8. https://doi.org/10.1007/S10554-021-02466-Y
30. Mach F, Baigent C, Catapano AL et al (2020) 2019 ESC/EAS Guidelines for the management of dyslipidaemias: lipid modification to reduce cardiovascular risk: The Task Force for the management of dyslipidaemias of the European Society of Cardiology (ESC) and European Atherosclerosis Society (EAS). Eur Heart J 41:111–188. https://doi.org/10.1093/eurheartj/ehz455
31. Grundy SM, Stone NJ, Bailey AL et al (2019) 2018 AHA/ACC/AACVPR/AAPA/ABC/ACPM/ADA/AGS/APhA/ASPC/NLA/PCNA Guideline on the Management of Blood Cholesterol: Executive Summary: A Report of the American College of Cardiology/American Heart Association Task Force on Clinical Practice Guidelines. J Am Coll Cardiol 73:3168–3209. https://doi.org/10.1016/J.JACC.2018.11.002
32. Orringer CE, Blaha MJ, Blankstein R et al (2021) The National Lipid Association scientific statement on coronary artery calcium scoring to guide preventive strategies for ASCVD risk reduction. J Clin Lipidol 15:33–60. https://doi.org/10.1016/j.jacl.2020.12.005